STUDY OF VOID EVOLUTION IN EPOXY RESIN DURING CURE

Kaitlin Rigitano[1], Andy George[2], Dan Rapking[1], G.P Tandon[1], Thao Gibson[1]
[1] Structural Materials Division, University of Dayton Research Institute, Dayton, OH
[2] Manufacturing Engineering Department, Brigham Young University, Provo, UT

ABSTRACT

It is well known that voids in composite materials lead to decreased structural performance. It is therefore necessary to understand their behavior in order to minimize the negative effects caused by the presence of these defects. In this work, an experiment was developed to study the evolution of voids in an epoxy material during cure. The experimental apparatus featured transparent glass tooling that allowed voids to be observed using an optical imaging setup under vacuum and elevated temperature conditions. Intentionally induced defects along with naturally evolving porosity were studied in both neat resin films and carbon fiber prepreg materials. Image analysis led to information on the evolution of void content, size, distribution, shape, and movement in an epoxy as a function of the cure cycle, and post-experiment optical microscopy provided insight into the morphology of defects that become trapped within composite materials during cure.

Corresponding author: Andy George, andy_george@byu.edu

1. INTRODUCTION

High performance structural composites have traditionally relied upon autoclave cure of prepreg materials to achieve the highest mechanical properties. Despite their promised advantages, many industry entities have been slow to switch from metals to composites. The major restraining factor has always been the cost and long cycle times to make the highest quality composites in such an autoclave-prepreg process. As the global aerospace market continues to become more competitive, and the automotive industry is constantly pushed to higher fuel economy standards, there is a strong push to develop less costly processes to make composites of similar quality. This is the driver behind out-of-autoclave (OoA) prepreg material systems in use or being developed today [1,2].

An OoA prepreg is designed with lower viscosity and other properties including dry areas to allow gas evacuation [3]. This allows better matrix saturation and degassing of the prepreg without resorting to an autoclave for consolidation pressure. Perhaps the greatest risk to using an OoA prepreg system is the reduced capacity of the manufacturing process to eliminate voids. Voids are any small bubble or pocket of air entrapped in the final cured laminate. These voids can originate in the prepreg manufacture, from handling the prepreg material including placement in the mold and ply stack-up [4], volatiles during cure, and any of several processing faults such as vacuum bag leaks [5].

Voids in composite laminates have a significant negative impact on the mechanical properties of parts [6-8]. For every 1% increase in void content between 0% - 5% yields a decrease in interlaminar shear strength and flexural strength of up to 10% and a decrease in flexural stiffness of up to 5% for every 1% of void content [9].

When the prepreg matrix is not yet gelled, these bubbles may be forced out of the system and to dissolve harmlessly into the resin by pressure. The pressure of an autoclave is usually sufficient to eradicate all voids. But an autoclave imposes significant costs in capital equipment, operation, and cycle time. A significant reduction in part cost can be afforded if the manufacturer can optimize a process enough to not need to resort to autoclave cure. For vacuum-bag-only (VBO) processing of OoA prepreg systems to meet autoclave-cured mechanical standards, the manufacturing process must be well understood in terms of how voids form and dissipate [10,11]. Yet most scientific literature on voids and prepreg discusses the final mechanical effects, as opposed to how to mitigate the voids outside of autoclave cure.

The objective of this work is to understand and capture void development/movement and/or resin movement during debulking/curing through high magnification imaging during the cure process. This was done in an attempt to identify differences that could equate to void evolution over time. Imaging experiments were able to capture visible changes in the voids during the course of the cure cycle.

2. EXPERIMENTATION

Experimentation was based on current literature that describes similar efforts [12-14]. In these experiments, an approximately 152 x 152 mm piece of 5320-1/IM7 prepreg was pressed against a 305 x 305 x 9.5 mm borosilicate glass sheet that had been previously cleaned and prepared with release agent (Figure 1). Some experiments also involved a 15 μm thick film of the same resin system used in the prepreg (Cycom 5320-1 epoxy) [15].

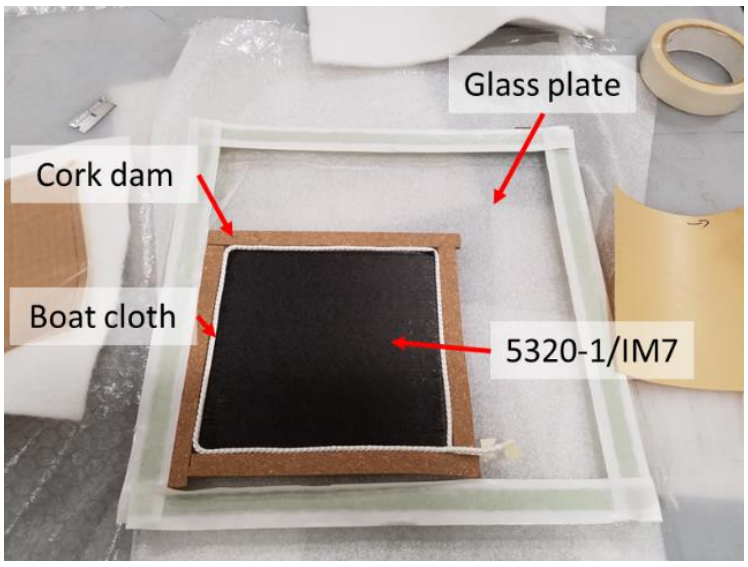

Figure 1. Prepreg on glass plate for void evolution experiments.

The manufacturer-recommended bagging sequence is shown in Figure 2. In this study, a fiberglass breather string and a 12.7 mm wide cork strip were used to replace the sealant tape and fiberglass cloth around the edges of the prepreg. For those experiments involving only resin film, a PTFE semi-permeable membrane was placed above the film, to allow gas evacuation without drawing the resin into the vacuum line.

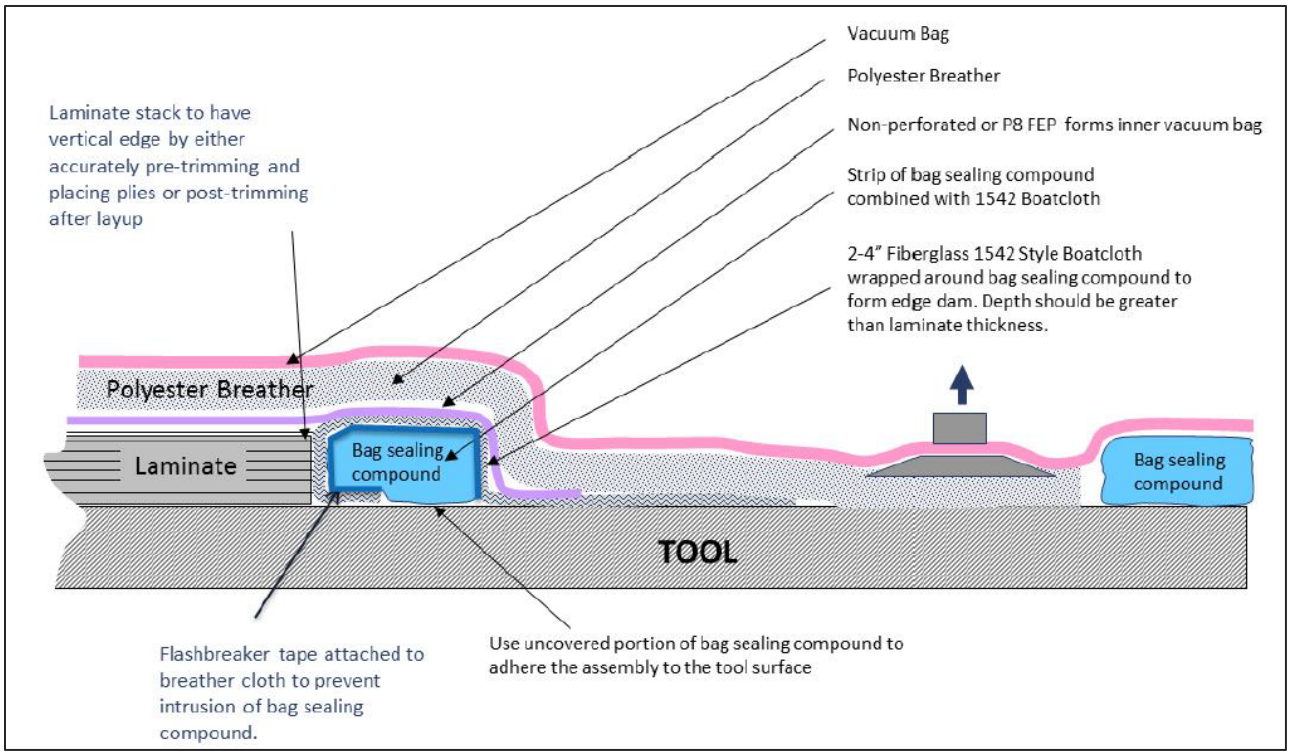

Figure 2. Manufacturer Recommended Bagging

A heating blanket was incorporated into the bagging scheme above the polyester breather layer, and an additional polyester breather layer was placed between the heating blanket and the vacuum bag. The heating blanket was connected to a Cole Palmer Digi-Sense Temperature Controller, and a thermocouple was placed inside the bag and connected to the temperature controller for temperature feedback (Figure 3). The bagged glass plate was elevated (glass plate facing downward) using lab stands, and a camera was placed underneath (Figure 4). The camera was a Point Grey 5-megapixel monochrome camera with a 180 mm focal length lens and a Fostec fiber light source. The camera was set up to image a 12 x 10 mm square in the corner of the prepreg sample, and captured an image every 30 seconds while the experiment was being conducted.

Table 1 lists the seven experimental infusions represented in this study designed to observe how voids evolve throughout a cure cycle. As seen, both prepreg and resin film were used in various combinations, and the film was sometimes punched with a needle to simulate voids and have more control over the initial conditions. For each laminate, full vacuum was applied initially (approximately 960 mbar vacuum pressure), and then the heating was begun. The "Full" cure cycle used for the majority of the experiments was: 1) ramp from ambient (approximately 28°C) to temperature T of 60°C at 1.1 °C/min, then 2) hold at 60°C for two hours, then 3) ramp at 1.1

°C/min to 120°C, then 4) hold at 120°C for 1 hour, before 5) cooling at 2.6 °C/min. These cure cycles are illustrated in Figure 5. Some experiments were conducted with an interrupted cure cycle. Cycle (A) followed the "Full" cycle except the second heating ramp proceeded only until 90°C, and then the heat was turned off and the laminate cooled naturally back to ambient. Cycle (B) only involved the first heating ramp, and only up to 47°C, whereupon the heat was turned off and the resin film cooled naturally back to ambient. These three cure cycle iterations are illustrated in Figure 5, as well as the viscosity profile accompanying the full cure cycle.

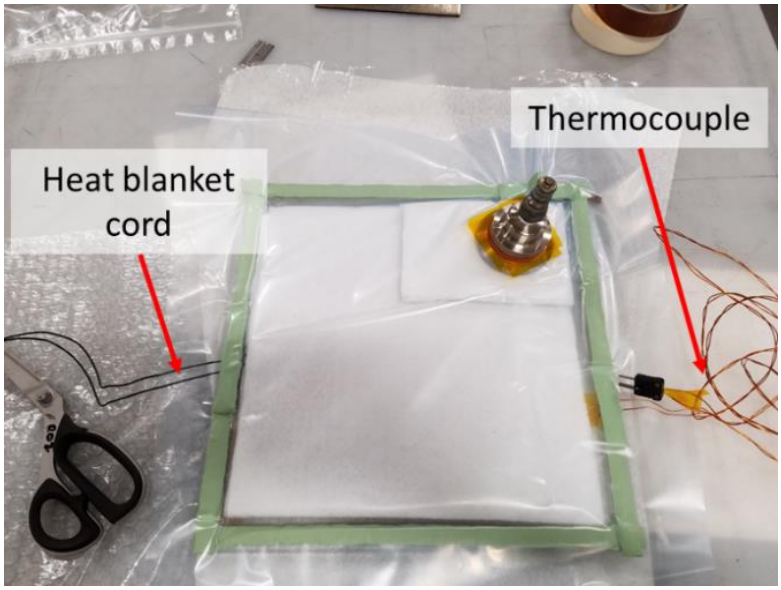

Figure 3. Prepreg was heated with a heat blanket connected to a temperature controller with a thermocouple as a temperature feedback.

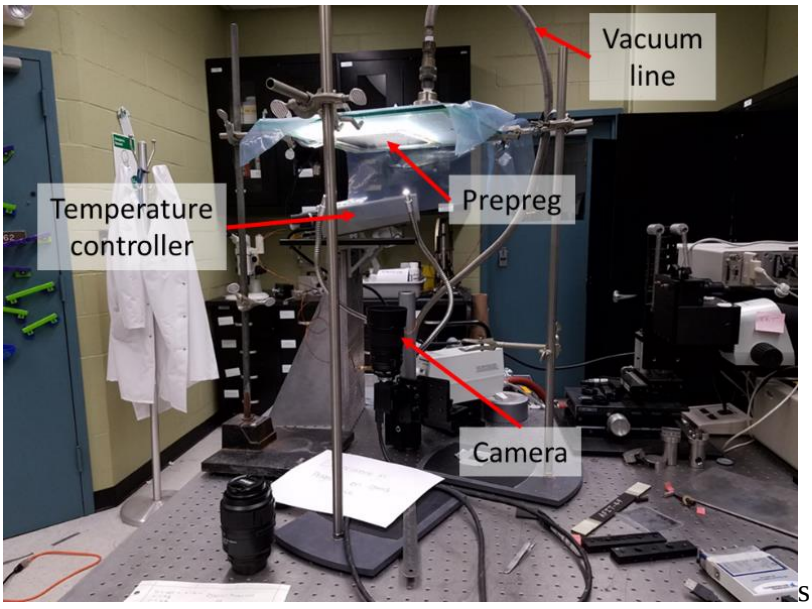

Figure 4. Prepreg/glass plate system was elevated above a camera for imaging while exposed to vacuum and a thermal cycle.

Table 1. Experimental program.

Experiment	Material	Cure
1	Prepreg	Full
2	Prepreg	Full
3	Prepreg	Interrupted (A)
4	Resin film only	Full
5	Resin film only	Full
6	Prepreg behind resin film with punched holes	Full
7	Resin film only, with punched holes	Interrupted (B)

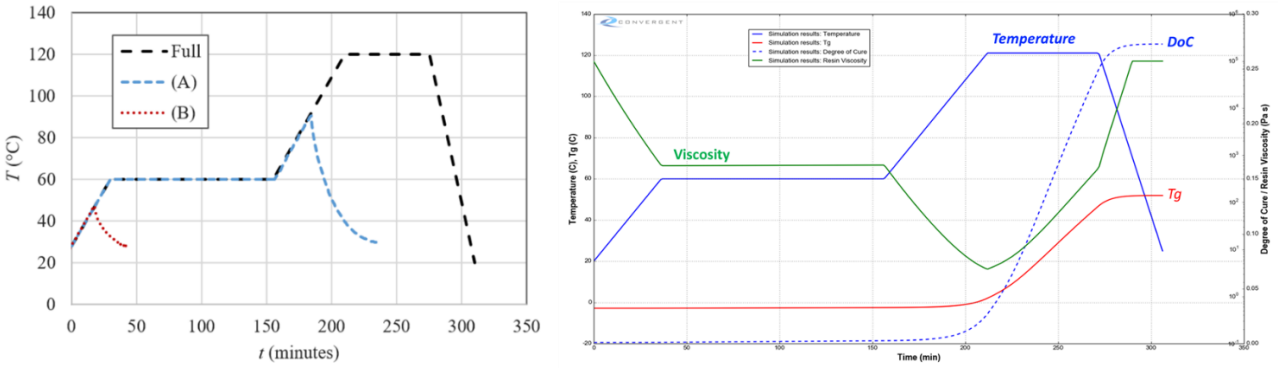

(a) (b)

Figure 5. (a) Temperature cycle used during cure and (b) viscosity profile during cure cycle

3. RESULTS

3.1 Prepreg voids qualitative analysis

Figure 6(a) shows the 12 x 10 mm image area of the prepreg at the start of experiment 1, before any vacuum or heat were applied. The image has a few scratch marks captured from the glass surface which can be seen as white streak lines. The prepreg itself appears rather dark as white light is not able to penetrate the opaque material. However, the faint outlines of individual fibers in the prepreg can be seen. Also seen in the image are white spots of varying shapes and sizes scattered widely across the image foreground.

As the focus of this study is the evolution of bubbles, the prepreg images captured during the cure cycle were modified by subtracting the binary initial image (6(a)) from all subsequent photos. An example image from the same experiment, at the end of the dwell at 60°C, is shown

in Figure 6(b), along with the modified image in Figure 6(c), after subtraction of image Figure 6(a). As seen in Figure 6(c), there are still a number of small white spots, which seem to be clustered into streaks which follow the fiber orientation.

To help identify the void features in these images, the last binary image for each experiment (captured after cooling back to ambient) was compared with micrographs of the cured laminate surface after removing it from the mold. Figure 7 shows this micrograph for experiment 1, focused on what looks like a long surface void, or a large area of dry fiber with droplets of resin within. Shown in the inset is the last image taken while still in the mold, where the long white streak is the only prominent feature, and matches in location with the long void from the post-cure micrograph. This suggests that the bright white spots are only reflections, from either small round voids, or resin droplets within a larger void like this streak. There were other, smaller surface voids seen in the post-cure micrograph, that were not immediately visible from the in-mold image, such as the four small white areas seen underneath the long surface void in the micrograph in Figure 7.

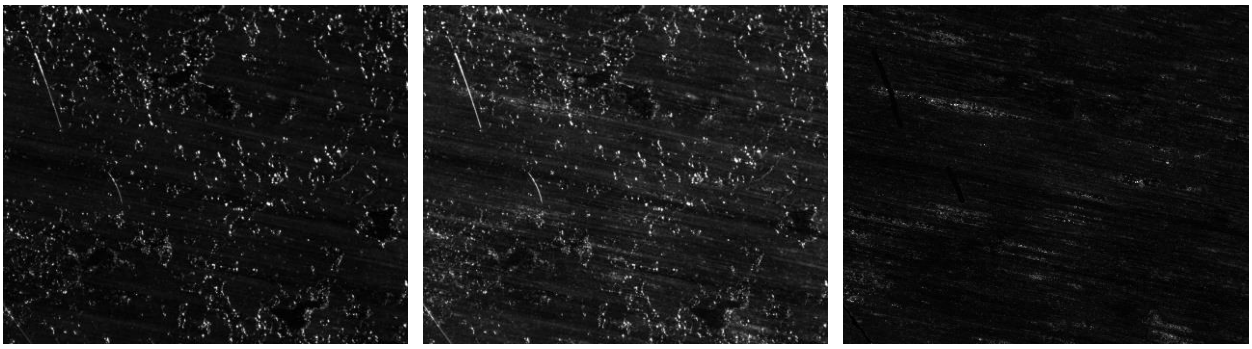

(a) (b) (c)

Figure 6. (a) Initial raw prepreg image before vacuum or heating; (b) raw prepreg image during cure experimentation; (c) image-b after subtraction of initial image-a.

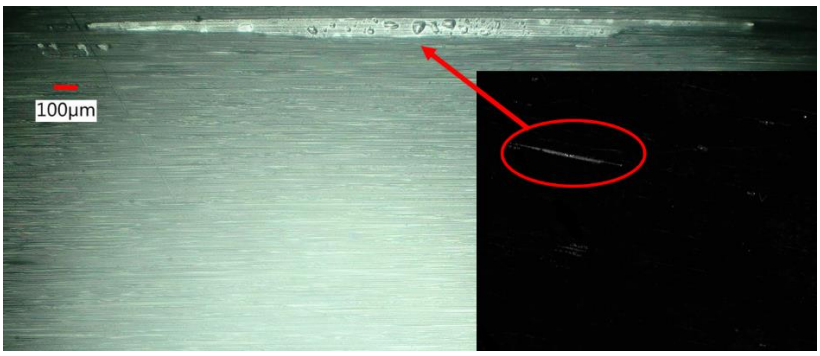

Figure 7. Post-cure micrograph of long surface void, with inset from last in-mold image taken for Experiment 1.

Figure 8 shows the last in-mold photograph for experiment 2, along with the entire corresponding 12 x 10 mm field of view in the post-cure micrograph. One long prominent void is visible in the bottom left of the in-mold image; gray-scale thresholding in image analysis, with a very low gray-level threshold makes other voids more clearly visible as well. In experiment 1,

the same low gray-level threshold was applied and automatically converted into a binary image for each original experimental image. For the other prepreg experiments, the lighting was non-uniform across the image, thus requiring image analysis filters (size and circularity after dilation and erosion cycles), combined with some manual marking of void features to identify the void features.

An example post-cure micrograph for each of the three prepreg experiments is shown in Figure 9 with a close-up of such surface voids. All of these voids run along the fiber direction and seem to push the fibers up away from the camera, which was placed underneath. The void content v_0 was calculated for the full field of view in the final experimental image, as the percentage of the total image area covered in void. The final v_0 was 0.6%, 4.0%, and 6.4% respectively for experiment 1, 2, and 3. The interrupted cure would intuitively leave more voids in the laminate than a full cure. But the cause for the discrepancy between the two full cure experiments (1 and 2) remains unknown. From a mechanical point of view, these void features are especially problematic as this concentration of the voids in a few long surface defects would most likely act as a discontinuity and crack initiation site during loading. It would be more preferential to mechanics, given the same v_0, if these voids were smaller and more spread out through the laminate.

(a) (b) (c)

Figure 8. (a) Post-cure micrograph for experiment 2, (b) last in-mold image, (c) mask showing voids.

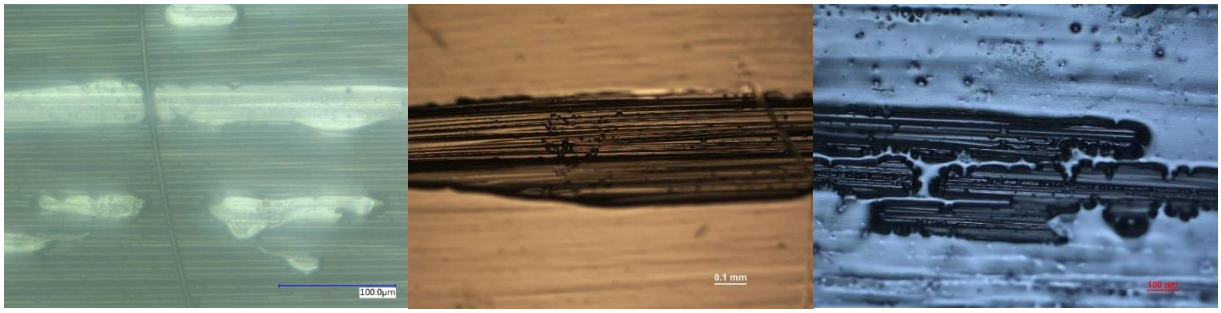

(a) (b) (c)

Figure 9. Post-cure micrographs of surface voids in prepreg experiments 1 (a), 2 (b), and 3 (c).

Another question is whether these voids result from 1) the as-supplied prepreg manufacture, 2) air entrapped when laying the prepreg on the glass mold, or 3) the cure cycle itself, e.g.

volatilization. Hamill, Centea, and Nutt published a recent study [4] showing the surface porosity in OoA prepreg is primarily from the second choice above, i.e. air trapped at the tool-prepreg interface during layup. Figure 10 presents void mask images for key moments in the experimental duration of each prepreg test, namely when the temperature first hits 60°C, then when it hit 120°C, then the last image i.e. after cool-down. Note that as experiment 3 involved an interrupted cure cycle and never was heated to 120°C, the corresponding image is absent. A significant amount of air was evacuated after the first heating ramp. Little volatilization is expected to occur at temperatures under 60°C, thus the left-hand images in Figure 10 should show nothing formed during processing.

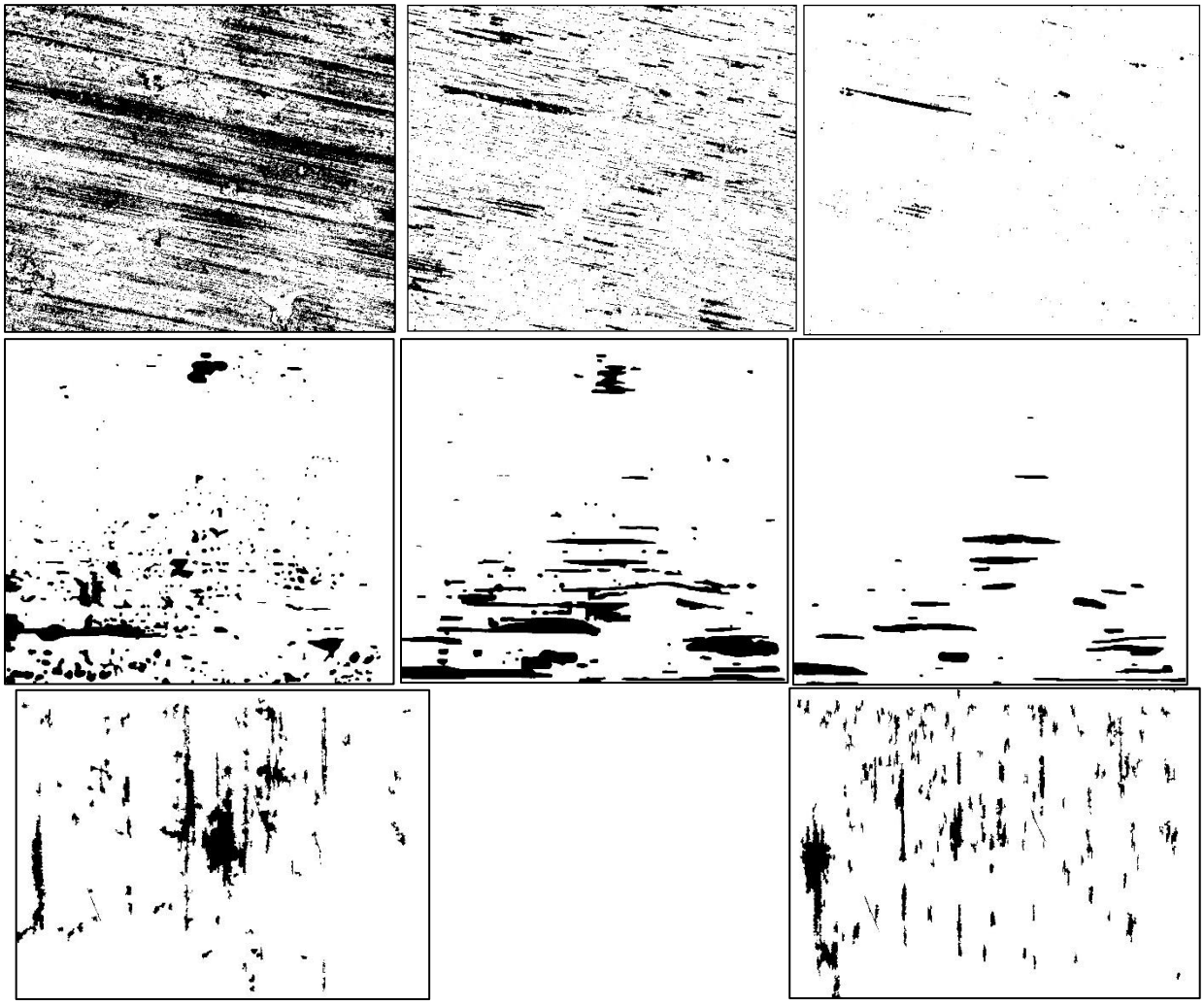

Figure 10. Void mask images (left = reach 60°C, mid = reach 120°C, right = end). Top row: experiment 1, mid row: experiment 2, bottom row: experiment 3 (no photo at 120°C).

In experiment 1, automatic thresholding showed many voids, both streaks and specks. Many of the long voids are gone after heating to 120°C, due to the increasing mobility of the bubbles as the viscosity decreased. Nearly all of the voids are gone by the end, with the main exception being the one long streak. This surviving long void appears to have been present in roughly the

same location in the first image. In fact, all voids appear to move little, only to dissipate in place as the air evacuation continues.

As already mentioned, the uneven shading made void detection more difficult. *A posteriori* shading correction attempts [16] were made to no immediate avail. Thus small thin voids as seen in experiment 1 were impossible to detect, since the boundaries of voids were more subjectively chosen during manual painting. The images in experiment 2 show similar trends however, with low- and high-void locations remaining constant throughout, i.e. little bubble mobility. Eventually only a few long streaks remain.

Experiment 3 shows much less void dissipation, most likely due to the interrupted cure cycle never allowing the low viscosities in the other experiments. There is some agreement between initial and final void locations, e.g. the large streak on the left-hand side. For both experiment 2 and 3, the long-skinny bubbles in the initial image seem to survive the cure cycle more than the rounder bubbles in the initial image. The rounder bubbles may be caused by air pockets trapped during placement of the prepreg upon the mold, while the longer bubbles may be from the prepreg manufacture, and somehow be more resistant to gas evacuation.

3.2 Prepreg voids quantitative analysis

Figure 11 shows the average area A, as well as the void content v_0 in select images from each of the prepreg experiments, along with the temperature histories. Note that the irregular shading in experiment 2 made void identification highly time-consuming for each image and therefore less images are recorded here. Both A and v_0 decrease sharply during the initial ramp to 60°C, then level off throughout the hold at 60°C. Experiment 1 showed a further decrease beginning roughly at the middle of the second heating ramp to 120°C, followed by a slight increase in A as most of the small voids disappear only leaving the one long streak (see Figure 10). Experiment 2 showed an increase in A but decrease in v_0 in the middle of the second heating ramp, again from disappearance of the smaller bubbles and leaving the larger bubbles. Experiment 3, with the interrupted cure cycle, begins to cool down at about the same temperature at which the changes occur in the other 2 experiments. It thus stays fairly constant in A and v_0. This data suggests that the initial heating ramp gets rid of most of the initial voids, due to the increased mobility of bubbles from the lower viscosity, although many persistent bubbles remain. Little happens during the two-hour hold at 60°C. A further significant increase in gas evacuation occurs during the second heating ramp from 60°C to 120°C, due to the even greater bubble mobility. The slight increase in v_0 in Experiment 1 during the hold at 60°C, and in experiment 3 near the end of heating are interesting behavior, and may be caused by volatilization before the heating ramp further mobilizes the remaining bubbles.

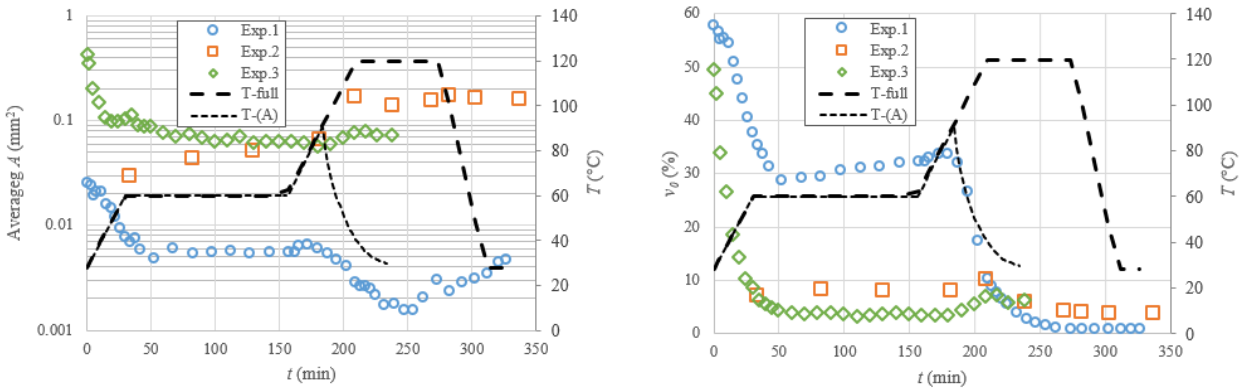

(a) (b)

Figure 11. (a) Average bubble area A and (b) void content v_0

Figure 12 shows the evolution of the aspect ratio φ averaged over all of the voids, calculated by dividing the major axis length by the minor axis length of a bounding ellipse around each void. An increase can be seen during the initial heating, especially in experiment 3, and then another increase during the second heating ramp to 120 °C, especially in experiment 2. This quantifies the observation made earlier that the rounder bubbles are degassed (evacuated) easier than the long skinny voids, causing the aspect ratio of the average bubble to increase.

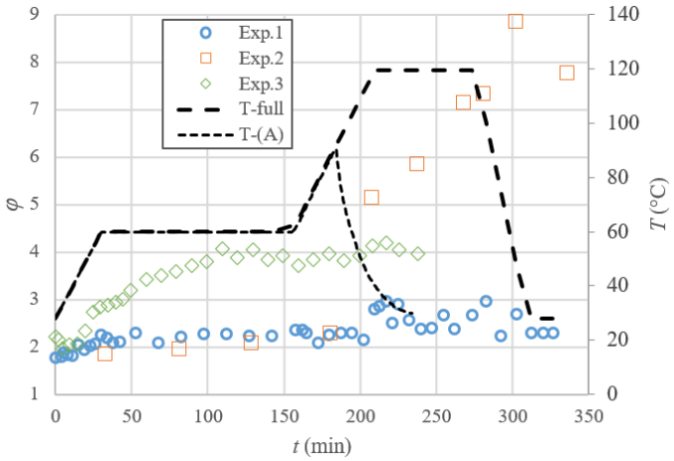

Figure 12. Average aspect ratio φ

Figure 13 illustrates an analysis of the relationship between a void and its neighboring voids, using two-point statistics [17,18]. These are color maps of the clustering of the bubbles, representing the average probability of finding another bubble a particular distance away from any given bubble placed in the middle of the color map image. One can see how initially the bubbles are spread across the image, with bubbles found in any direction. But later on in the experiment the bubbles become more clustered into a streak, where there's little probability of finding a bubble outside of the streak in any direction. These color maps result from experiment 1, but similar clustering behavior was seen in the other two prepreg experiments.

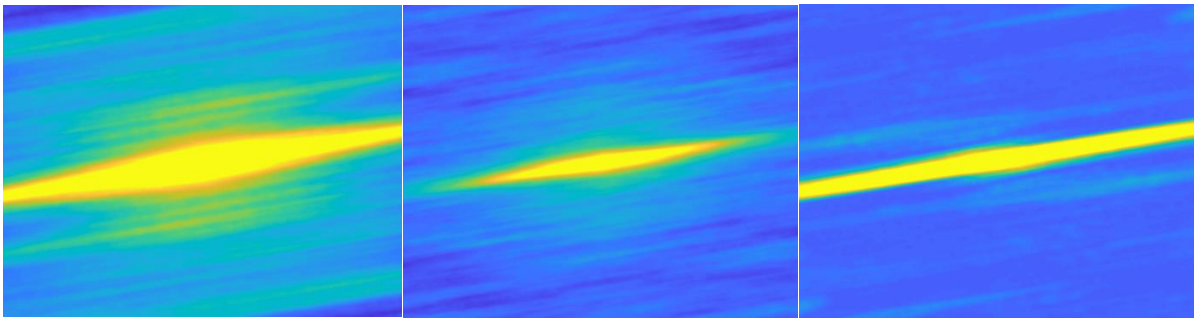

(a) (b) (c)

Figure 13. Two-point statistical maps denoting void clustering for experiment 1: (a) = reach 60°C, (b) = reach 120°C, (c) = end

3.3 Resin film voids qualitative analysis

The fibers in the prepreg cause the voids to be long and stringy, and more difficult to identify and characterize than the usual rounder bubbles in a non-fibrous medium. To better see the effect of the cure cycle on bubbles without the complication of the fibers, various experiments were also performed with thin layers of neat resin film.

Experiment 4 was the first of these, and showed a surface filled with bubbles initially, presumably from all the air entrapped when placing the film on the glass surface. As it heated up, the resin appears to liquefy, leaving bubbles floating as islands in the resin, which appear to be coagulated air in the form of voids. The mold appears to have had enough deviation from flatness, that the bubbles moved with gravity towards a corner of the field of view, thus the bubble distribution is not what it would naturally be. The increasing temperature evacuates the voids more easily than in the prepreg because of the lack of fibers which act as filter impediments to bubble evacuation. The voids are also larger and rounder than in the prepreg experiments, again due to the lack of fibers to constrain the bubbles to conform to the thin inter-fiber gaps.

Experiment 5 was performed similarly, but the experiment setup was leveled to help prevent resin flow due to gravity. Hundreds of bubbles are in in the initial images, barely visible against the cross-hatch pattern of the PTFE membrane (Figure 14). Although more flat, with less obvious directionality to the movement, these bubbles are more mobile than in the prepreg experiments, and they are evacuated quickly through the porous membrane, with no bubbles visible after reaching 120°C.

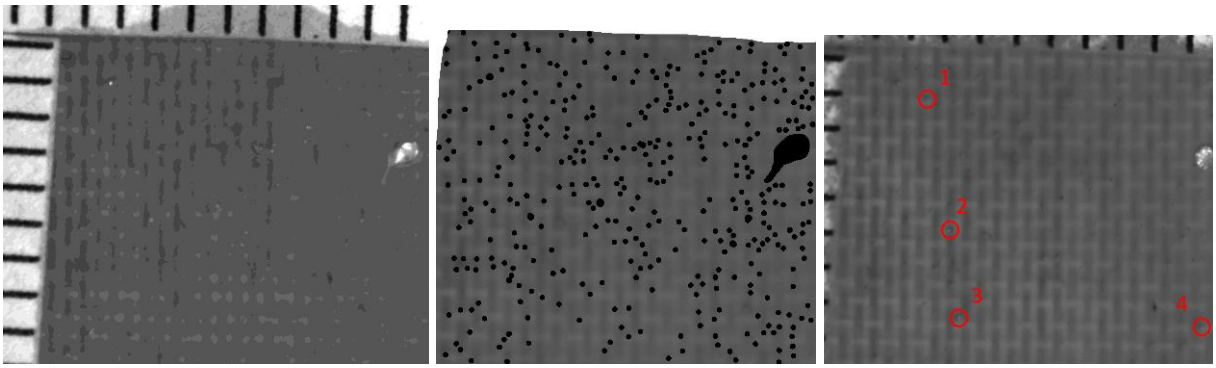

(a) (b) (c)

Figure 14. (a) Experiment 5 image at beginning of hold at 60°C, (b) with marked locations of voids, and (c) image at end of hold at 60°C. Black tick marks near the image edges represent mm spacing.

To evaluate the evolution of these bubbles, an image at the end of the hold at 60°C was selected, and four of the most prominent bubbles were identified (Figure 14 (c)). These holes were then identified in images before and after. At the beginning of the experiment, there was a tiny mark for each of these four bubbles, and all four increase in size during the heating ramp to 60°C when the original image was taken. This increase in size is possibly from air coming out of the liquefied resin with the vacuum application, but the cause is unknown. Little change occurs throughout the 60°C hold. During the second ramp, these four along with all other bubbles disappear. Some voids move to the right out of the field of view, but most simply shrink to nothing, presumably by gas evacuation through the membrane.

Large voids were purposefully introduced into the other resin film experiments, to allow larger and more-pronounced features to follow during void evolution through the cure cycle. This was done with by punching 250 to 950 μm diameter holes in the film with various sized needles. Experiment 6 was the first with punched holes, and was performed with a layer of prepreg behind the film. This served two purposes: 1) to give a dark background against which voids were easier to automatically identify than against the membrane cross-hatch pattern, and 2) so that the gas evacuation was forced through prepreg instead of simply a PTFE membrane and would thus be possible more similar to the prepreg experiments. But the opaque prepreg layer also darkened the images which again required low gray-level thresholding to see any of the voids, and made it impossible to see any of the faint small bubbles seen in the experiments 4 and 5.

Figure 15 illustrates the punched hole pattern for experiment 6, and their location in the initial mask image showing the punched holes. With vacuum and heat, the voids begin to evolve in both size, shape, and location (Figure 16). The ramp to 60°C again causes most of the air to be degassed, followed by stagnant behavior again in the hold at 60°C. The ramp to 120°C causes further degassing and alignment of the bubbles with the direction of the fibers in the adjacent prepreg layer, presumably as these large degas-resistant bubbles are drawn through the prepreg for evacuation. By the end of the dwell at 120°C, most of the air in these elongated bubbles has

been pulled through, and at the end of the experiment, there is little left of only one of the original 12 tracked voids.

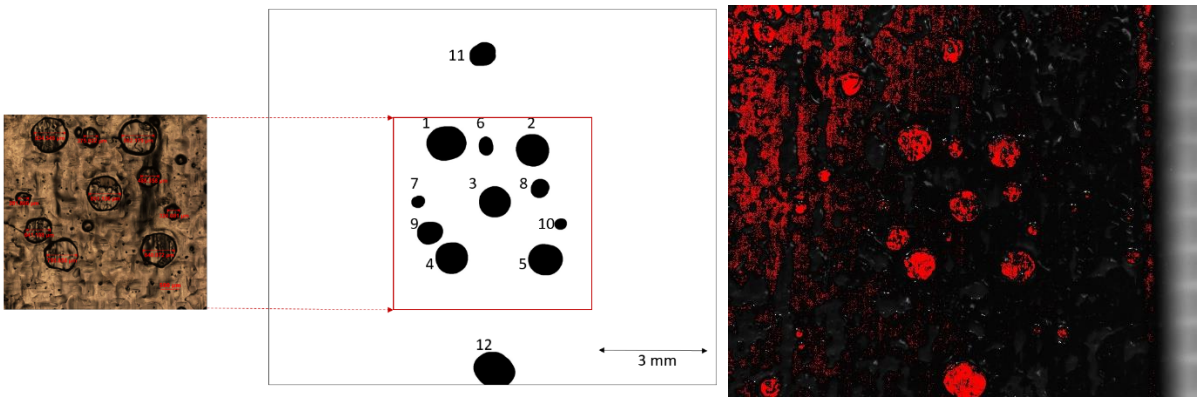

(a) (b)

Figure 15. (a) Experiment 6 punched hole pattern, and (b) their identification by gray-level thresholding in the initial image.

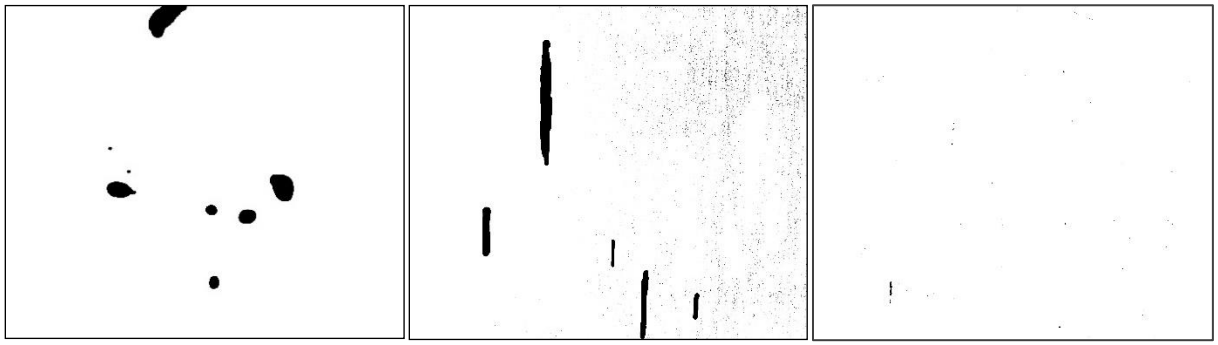

(a) (b) (c)

Figure 16. Experiment 6 void mask images: (a) = reach 60°C, (b) = reach 120°C, (c) = end

In the last experiment (7), five holes were punched in the film but no prepreg was used. The cure cycle was interrupted with very little heating, only ramping to 47°C before allowing to cool naturally. The limitation on temperature and thus high viscosity limit degassing, and many voids remain in the image at the end of the experiment, although in much smaller sizes. The punched holes and five more prominent voids from the initial image were again tracked through the experiment, and the resulting masks of the first and last image are shown in Figure 17. The voids in the last image are difficult to see due to their small size. They have not moved in location much, but have greatly decreased in size through the heating ramp, as short as it was. This again shows how much of the void evacuation is accomplished by the first heating ramp.

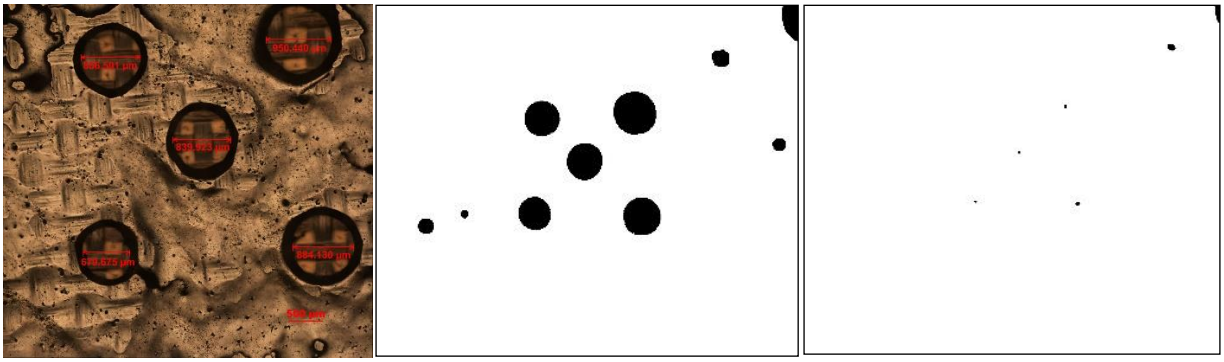

(a) (b) (c)

Figure 17. (a) Experiment 7 punched hole pattern, and (b) first and (c) last mask images showing the five punched holes in addition to five prominent voids.

3.4 Resin film voids quantitative analysis

Quantitative analysis of the film experiments was complicated by the image background. The voids in experiment 4 were hand-painted due to the difficulties with automated void detection arising from the membrane's cross-hatch pattern (Figure 14). The voids in experiment 5 were more numerous, and had fainter outlines exacerbating the challenges. Without clear outlines, the shape of the bubbles was also impossible to characterize, except for one particularly large void, visible on the far right side of Figure 14(a). Thus each void in select images was simply marked for distribution and total bubble count studies (Figure 14). Experiment 6 proved to be too dark to allow for any kind of detection of the many small bubbles in these images, and thus no quantitative results are available. Figure 18 plots the total bubble count for experiments 4 and 5, showing a roughly linear decrease for experiment 5, down to essentially 0 by the end of the ramp to 120°C.

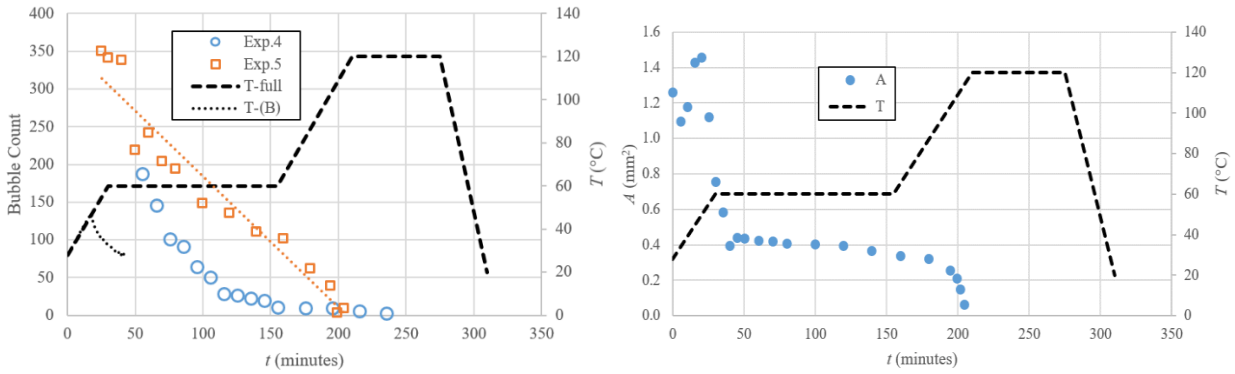

(a) (b)

Figure 18. (a) Total bubble count for experiment 4 and 5 and (b) largest bubble area in experiment 5

The area of the one large irregularly shaped bubble in experiment 5 was measured and the results are also shown in Figure 18. The area of the bubble drops rapidly during the ramp to 60°C, then

stays more constant (with a steady slight decrease) throughout the dwell at 60 °C. The area decreases faster and faster once the second temperature ramp from 60°C to 120°C begins, and the bubble is gone by the time the temperature reaches 120°C.

Experiment 7, although challenged by the membrane cross-hatch background (Figure 19), had the best focus of the film experiments, and thus was targeted for a machine learning (ML) based attempt at automated void detection of the hundreds of bubbles in each image. This was accomplished using Mask R-CNN [19] as implemented in "detectron2" an open source object detection library developed by Facebook AI Research [20]. Mask R-CNN is a deep neural network that identifies objects of interest and produces corresponding segmentation masks [19]. A Python script was built to generate masks as well as train/retrain the model to fit the data sets. Figure 19 shows an example image overlaid with the ML results for the first image, in which the five punched holes are clearly visible. Figure 19 also shows two resulting mask images, the one corresponding to the same initial image, and the one from the very last image, showing a scattered distribution of small bubbles.

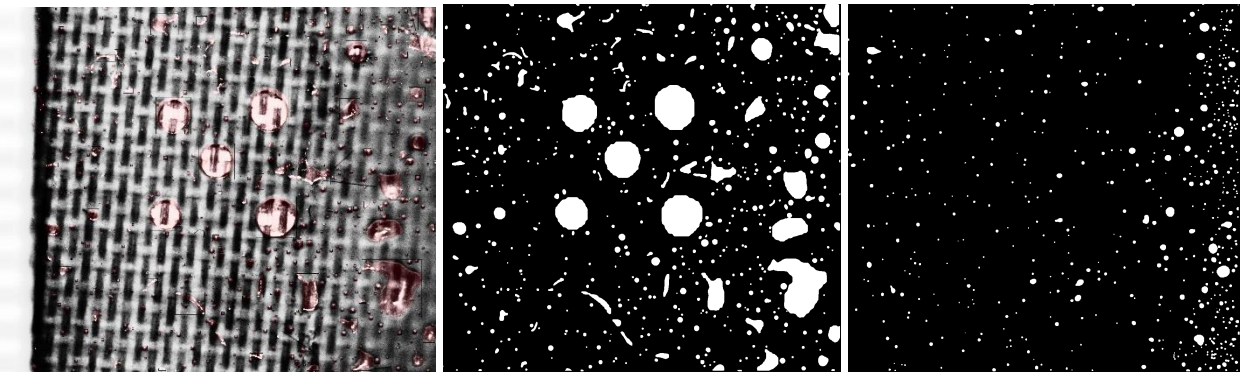

(a) (b) (c)

Figure 19. (a) Machine learning void identification overlay and (b) resulting mask image for experiment 7's initial image, and (c) resultant final mask image.

Figure 20 shows the two-point statistics for Experiment 7: the initial image, when the heat is turned off at 47°C, and the final image after reaching ambient temperature. The clustering initially shows the cross-pattern distribution of the five punched holes as they are by far the largest voids. These punched holes decrease in size and during the heating ramp, and the distribution ends up as scattering of many very small voids at the end.

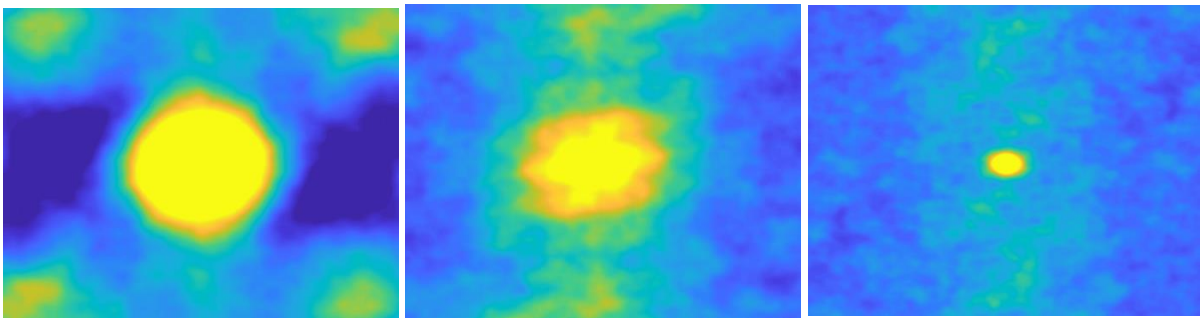

(a) (b) (c)

Figure 20. Two-point statistical maps denoting void clustering for experiment 7: (a) = initial, (b) = start cooling, (c) = end

Figure 21 plots the average area, void content, bubble count, and aspect ratio throughout the short cure cycle. The temperature profile is overlaid on these graphs without a scale, only to show the time-position of the end of heating. As seen, average A and v_0 follow an identical trend, as the number of bubbles stays around 530. Both decrease quickly, then level off as the heating ends and the sample cools down, slowing gas evacuation due to rising viscosity. The void content drops from 12% initially to approximately 2% in this short and interrupted cure cycle. The aspect ratio drops slightly, meaning the bubbles become rounder until the heating ends and then they level off.

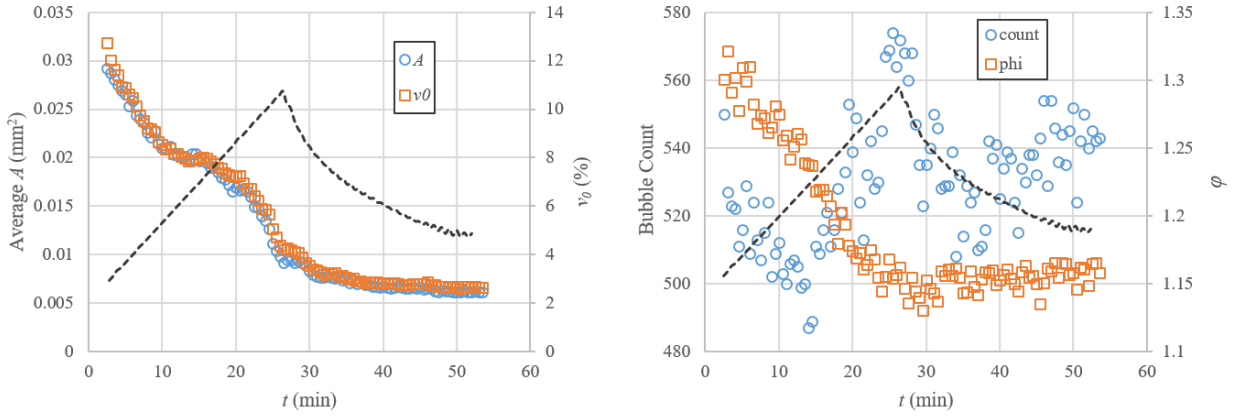

(a) (b)

Figure 21. (a) Average area, void content, (b) bubble count, and aspect ratio

4. CONCLUSIONS

The cure of both prepreg and epoxy film was monitored by imaging the evolution of voids throughout both full and interrupted cure cycles. In prepreg, there is a significant amount of trapped air at the beginning of the cure cycles. Through an initial ramp to 60°C, most of this air is evacuated through the breather cloth to the vacuum. Little degassing occurs over the hold time at 60°C. A further, smaller reduction in void content occurs during the second ramp from 60 to 120°C. Long skinny voids are common, as constrained by the fibers, some of which remain

through the entire cure cycle and seem resistant to degassing. In films, a similar pattern is observed, where most of the degassing occurs in the first heating ramp, and little beyond that until the second heating ramp.

There are unique challenges to identifying voids in each of the experimental iterations. Manual identification, automated grey-level thresholding, various image analysis tools, and a machine learning script were all used to assist in gathering the data for this analysis.

5. ACKNOLWEDGEMENTS

The authors are grateful to Floid Gilbert for performing the machine learning bubble detection scripts used in the film-only experiment. Additionally, the authors would like to acknowledge our sponsor, Advanced Computational Technology, LLC, for this work performed under contract 16-ACT-2018-001-UDRI, and AFRL SBIR contract FA8650-18-C-5004, program manager Dr. Rick Hall of AFRL/RXCC. The information in this paper was approved for public release, distribution unlimited by 88ABW-2020-1145.

6. REFERENCES

1. Gardiner, G. “Out-of-autoclave prepregs: hype or revolution?” High Perform Compos (2011).
2. Centea, Timotei, Lessa K. Grunenfelder, and Steven R. Nutt. "A review of out-of-autoclave prepregs–Material properties, process phenomena, and manufacturing considerations." Composites Part A: Applied Science and Manufacturing 70 (2015): 132-154.
3. Ridgard, C. “Out of autoclave composite technology for aerospace, defense and space structures.” Proc SAMPE 2009 conf. Baltimore, MD, 2009.
4. Hamill, L, Centea, T., and Nutt, S. "Surface porosity during vacuum bag-only prepreg processing: Causes and mitigation strategies." Composites Part A: Applied Science and Manufacturing 75 (2015): 1-10.
5. Centea, T., and Hubert, P. "Out-of-autoclave prepreg consolidation under deficient pressure conditions." Journal of Composite Materials 48.16 (2014): 2033-2045.
6. Olivier, P., Cottu, J., and Ferret, B. "Effects of cure cycle pressure and voids on some mechanical properties of carbon/epoxy laminates." Composites 26.7 (1995): 509-515.
7. "Composite Materials Handbook," MIL-HDBK-17-3F. Department of Defense, 3(5) (2002)
8. L. Ling, B. Zhang, D. Wang and Z. Wu. "Effects of Cure Cycle on Void Content and Mechanical Properties of Composite Laminates." Composite Structures 73 (2006): 303-309.
9. Ghiorse, S. R. "Effects of Void Content on the Mechanical Properties of Carbon/Epoxy Laminates." SAMPE Quarterly 24(2) (1993): 54-59.
10. Lucas S, Howard S, Senger J. Vacuum bag only processing: improving prepreg out-time and porosity for large composite structure. Proc SAMPE 2010 conf. Seattle, WA, 2010.

11. Sutter JK, Kenner WS, Pelham L, Miller SG, Polis DL, Hou T, et al. Comparison of autoclave and out-of-autoclave composites. Proc 42nd int SAMPE tech conf. Salt Lake City, UT, 2010.
12. Helmus, R. et al. “An experimental technique to characterize interplay void formation in unidirectional prepregs.” *Journal of Composite Materials* 51(5) (2017): 579-591.
13. Hu, W. et al. “In situ monitoring and analysis of void evolution in unidirectional prepreg.” *Journal of Composite Materials* 52(21) (2018): 2847-2858.
14. Gangloff, J. et al. “Entrapment and venting of bubbles during vacuum bag prepreg processing.” *Journal of Composite Materials* 51(18): (2017), 2757-2768.
15. https://www.solvay.com/en/product/cycom-5320-1#product-documents (2020)
16. Bonnet, N. “Shading correction (a posteriori).” UMRS-INSERM (Reims, France) https://imagej.nih.gov/ij/plugins/inserm514/Documentation/A_posteriori_shading_correction_514_v3/A_posteriori_shading_correction_514_v3.html, (2020).
17. Fullwood, D., D. Gerrard, A. George, & D. Halverson. “Dispersion metrics for composites – a machine learning based analysis.” Proceedings of SAMPE International Conference, Long Beach, USA, 2013.
18. Niezgoda, S., Fullwood, D., and Kalidindi, S. “Delineation of the space of 2-point correlations in a composite material system.” *Acta Mater* 56 (2008): 5285–5292.
19. He, Kaiming, et al. "Mask r-cnn. corr abs/1703.06870 (2017)." arXiv preprint arXiv:1703.06870, https://dblp.org/rec/bib/journals/corr/HeGDG17, (2017).
20. Wu, Y. et al. “Detectron2.” https://github.com/facebookresearch/detectron2, (2019).